PERGAMON

Journal of Atmospheric and Solar-Terrestrial Physics 62 (2000) 311–322

Journal of ATMOSPHERIC AND SOLAR-TERRESTRIAL PHYSICS

Non-stationary Alfvén resonator: vertical profiles of wave characteristics

K. Prikner[a], K. Mursula[b,*], F.Z. Feygin[c], J. Kangas[b,d], R. Kerttula[b], T. Pikkarainen[b], O.A. Pokhotelov[c], V. Vagner[a]

[a]*Geophysical Institute, Academy of Sciences of the Czech Republic, Bocní II, 14131 Praha 4, Sporilov, Czech Republic*
[b]*Department of Physical Sciences, University of Oulu, FIN-90014, Oulu, Finland*
[c]*United Institute of Physics of the Earth, Russian Academy of Sciences, Bolshaya Gruzinskaya 10, 123810 Moscow, Russia*
[d]*Sodankylä Geophysical Observatory, University of Oulu, FIN-99600, Sodankylä, Finland*

Received 8 April 1999; received in revised form 8 November 1999; accepted 22 November 1999

Abstract

A Pc1/IPDP event recorded by the Finnish search coil magnetometers on 15 December 1984 was analyzed in a companion paper (Mursula et al., 2000. Non-stationary Alfvén resonator: new results on Pc1 pearls and IPDP events. J. Atmos. Solar-Terr. Phys. 62(4), 299–309) using numerical simulations of the ionospheric Alfvén resonator (IAR). EISCAT incoherent scatter radar data were used to determine the vertical profiles of ionospheric plasma parameters. In this paper, the detailed altitude profiles of several wave characteristics at the IAR eigenfrequency are computed up to 1000 km height, including, e.g., the real normalized amplitude of the magnetic wave field component, ellipticity and orientation of the polarization ellipse in the horizontal plane. We also calculate the altitude profile of the energy flux density (Poynting vector). These features illustrate in detail the ionospheric effects on the wave spectral structure in a non-stationary IAR, and their significance in the formation of the Pc1/IPDP signal on the ground.

1. Introduction

The special type of geomagnetic pulsations called IPDP, depicting a diminishing wave period, has been studied for many years. It is known that IPDPs occur mostly in the evening–midnight sector of the magnetosphere and their occurrence is related to the non-stationary substorm processes in the magnetosphere and ionosphere. IPDP events last usually for half an hour to one and a half hour (Heacock, 1973; Maltseva et al., 1979; Kleimenova et al., 1995). According to Kleimenova et al. (1995), an ionospheric trough is often seen above the region of IPDP observation.

The generation mechanisms of IPDPs have so far only taken into account the magnetospheric aspects of generation, e.g., the azimuthal and radial drifts of energetically charged particles across the magnetic field during the substorm development (Heacock, 1973; Kangas et al., 1974; Guglielmi, 1974; Koleszar, 1989; see also the review by Kangas et al., 1998). However, because the ionosphere plays a significant role for ground-based observations of ion cyclotron waves, the IPDP theories including only the magnetospheric processes are not expected to describe completely the IPDPs observed on the ground. Indeed, so far no

* Corresponding author. Tel.: +358-8553-1366; fax: +358-8553-1287.
E-mail address: Kalevi.Mursula@oulu.fi (K. Mursula).

1364-6826/00/$ - see front matter
PII: S1364-6826(99)00126-1

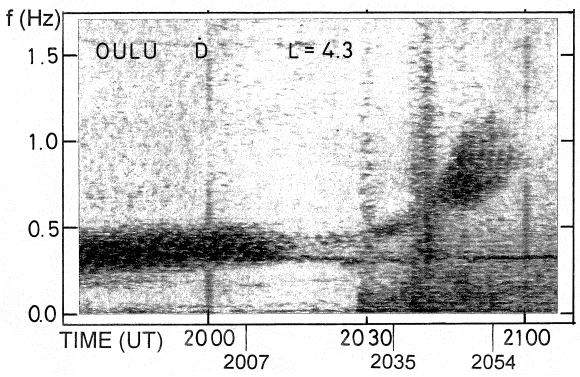

Fig. 1. Frequency–time display of the IPDP event on 15 December 1984, recorded at Oulu, Finland. Three vertical lines indicate the times for which the resonator properties have been calculated.

direct observations of the frequency rise during a ground-based IPDP event have been made in space by satellites (see, e.g., Bossen et al., 1976).

In a companion paper (Mursula et al., 2000; to be called P1), we have analyzed a structured Pc1 event of 15 December 1984, which, after a substorm onset, evolved into a structured IPDP event. Using simultaneous measurements of ionospheric parameters by the EISCAT radar, we calculated the reflection and transmission coefficients of Pc1/IPDP waves in the ionospheric resonator. We showed that the wave frequency observed on the ground corresponds to the frequency of the maximum of the transmission coefficient, i.e., the eigenfrequency of the resonator (Lysak, 1991, 1993). The calculated eigenfrequency could be increased during the event so as to match the frequency rise observed during the IPDP phase. We suggested in P1 that the ionosphere has an active role for Pc1/IPDP waves observed on the ground and that the IPDP signal is a combined effect of the frequency rise in the magnetospheric wave source and the simultaneous increase in resonator eigenfrequency.

In this paper, we present a detailed analysis of the method used in P1. Moreover, a complete altitude profile of the wave properties (e.g. amplitude, polarization and energy flux) inside the ionosphere resonator has been calculated.

2. The numerical method

The principle of a numerical calculation of the total wave field at any ionospheric altitude, generated by

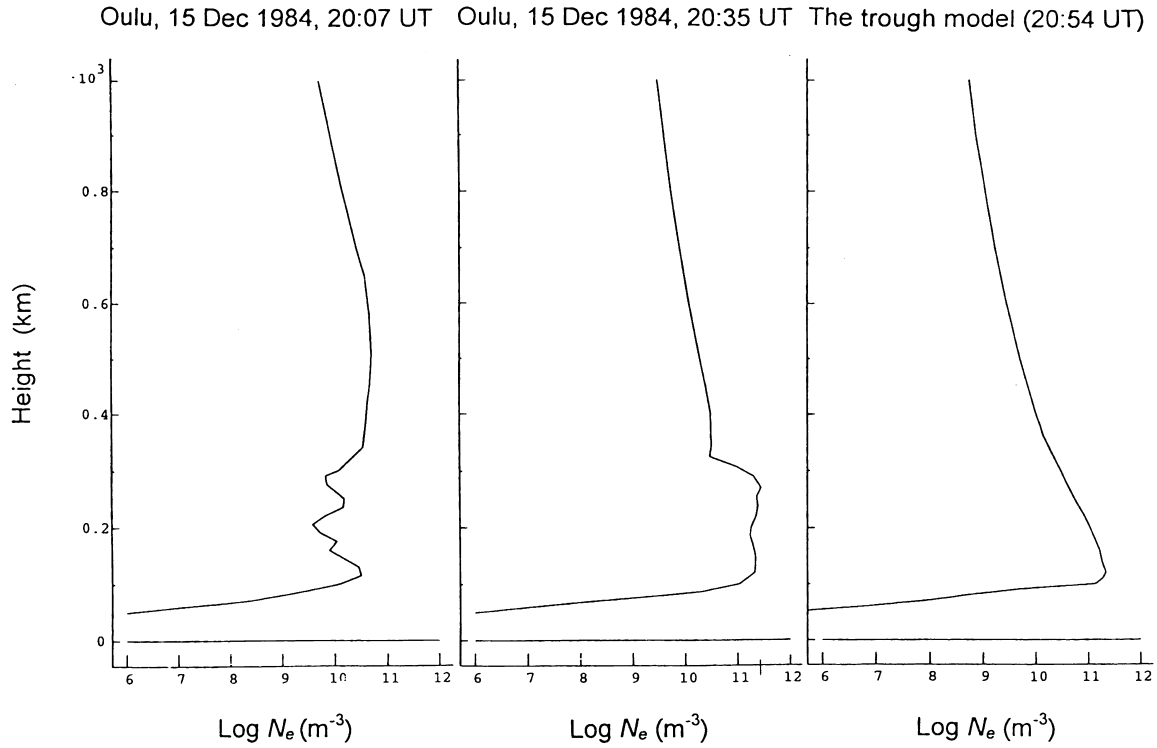

Fig. 2. The three altitude profiles of the electron densities (N_e). Two first profiles at 2007 and 2035 UT are based on EISCAT measurements at altitudes below 300 km, the profile at 2054 UT is a model profile fit to match the observed wave frequency.

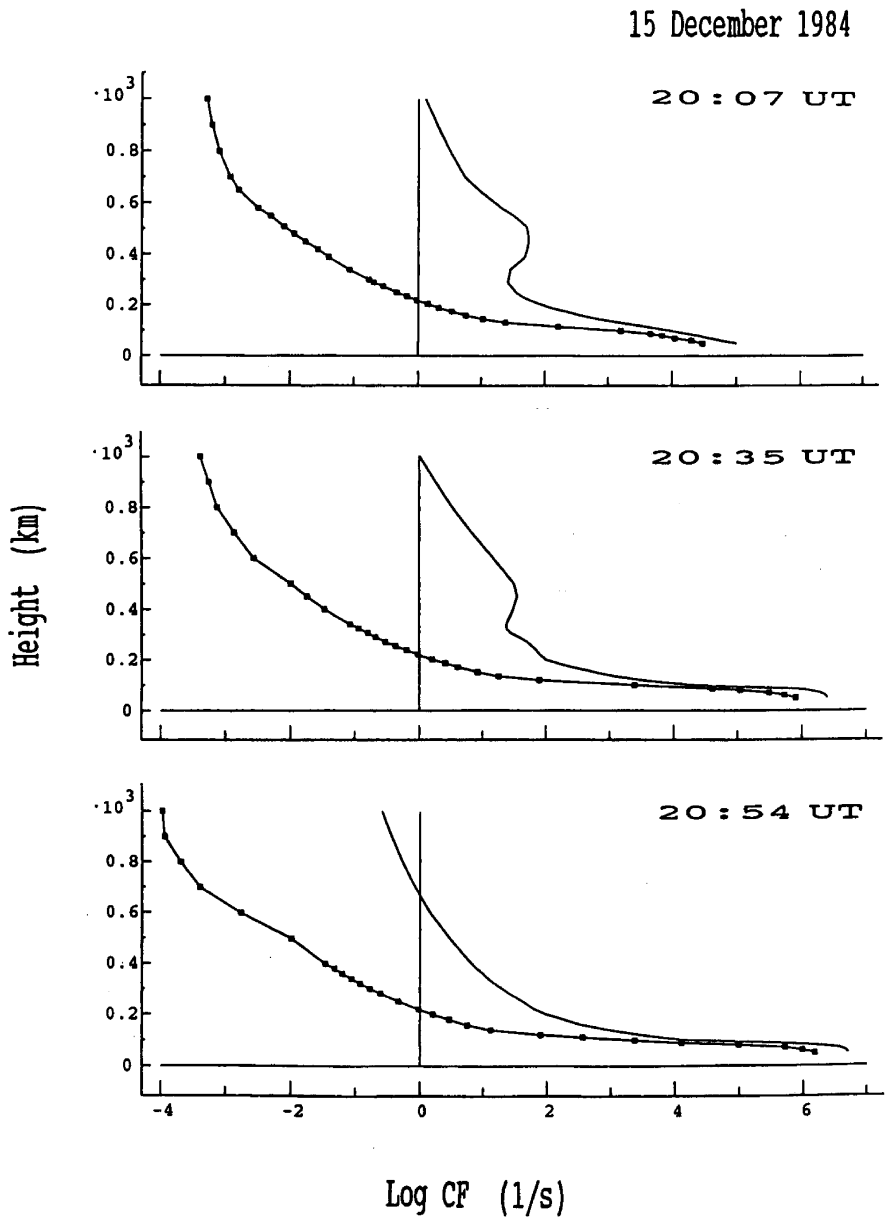

Fig. 3. The altitude profiles of electron (smooth line) and ion (smooth line with marks) collision frequencies for the three times.

ULF signal incident from above on the ionosphere, was outlined by Prikner and Vagner (1991). The ionosphere is described as a stratified, inhomogeneous, anisotropic (magnetized) and dissipative medium with a two-component plasma (electrons and ions, $N_e = N_i$), and the characteristics of the medium are taken to vary along the vertical z-axis only (Vagner, 1982; Prikner and Vagner, 1983). Dissipation is characterized by the effective collision of electrons (collision frequency ν_e) and ions (ν_i) with the neutral particles in the medium. The anisotropy is due to the presence of the external geomagnetic field $\mathbf{B}_0(z)$, which is treated in the dipole field approximation. The ionospheric transition layer and the layer of non-ionized atmosphere are bounded from below by the Earth's surface with a homogeneous specific conductivity σ_E.

Wave propagation through the ionosphere has been modeled assuming a homogeneous plane wave mode (**L**- or **R**-polarization) of a given frequency f and wave vector **k** incident upon the upper boundary of the ionosphere, in the plane of the dipole magnetic field meridian. **L**-polarization is counterclockwise, when

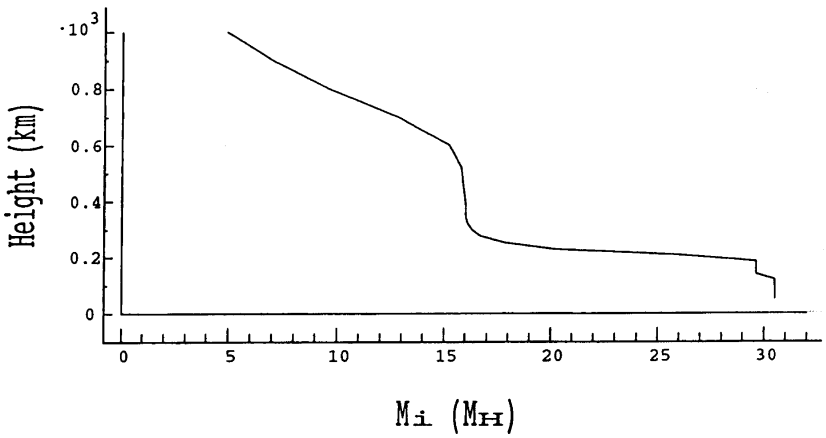

Fig. 4. The altitude profile of the effective ion mass (in units of proton mass) used in numerical calculations.

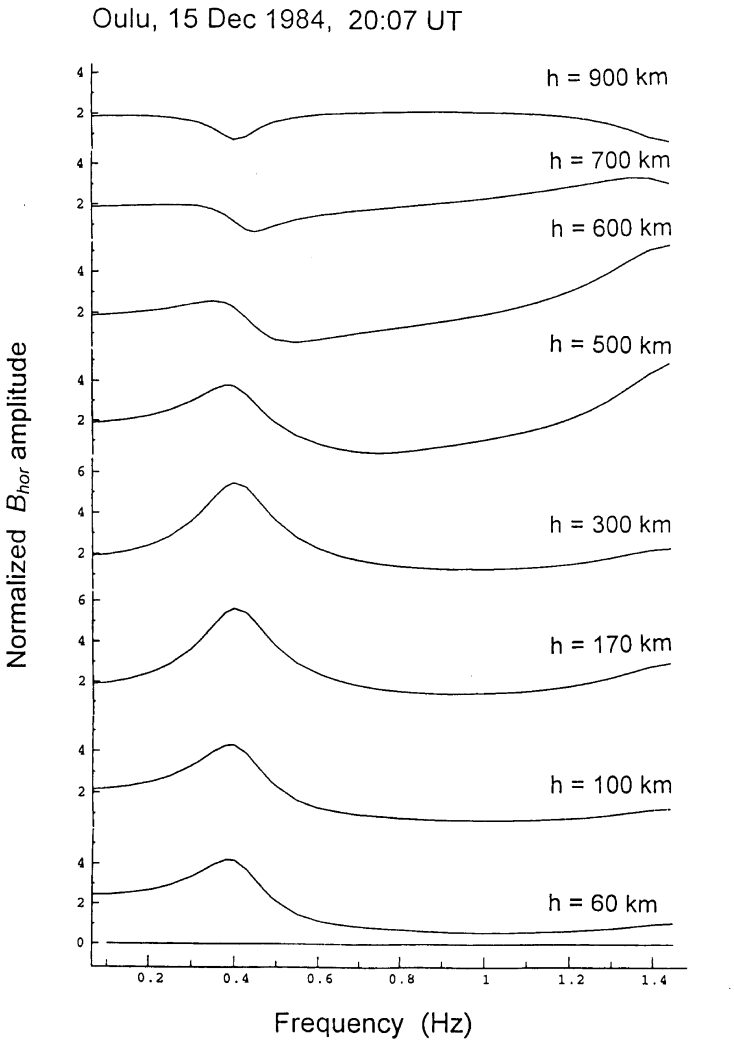

Fig. 5. Frequency dependence of the normalized horizontal wave amplitude at different altitudes for: (a) 2007 UT, (b) 2035 UT, and (c) 2054 UT.

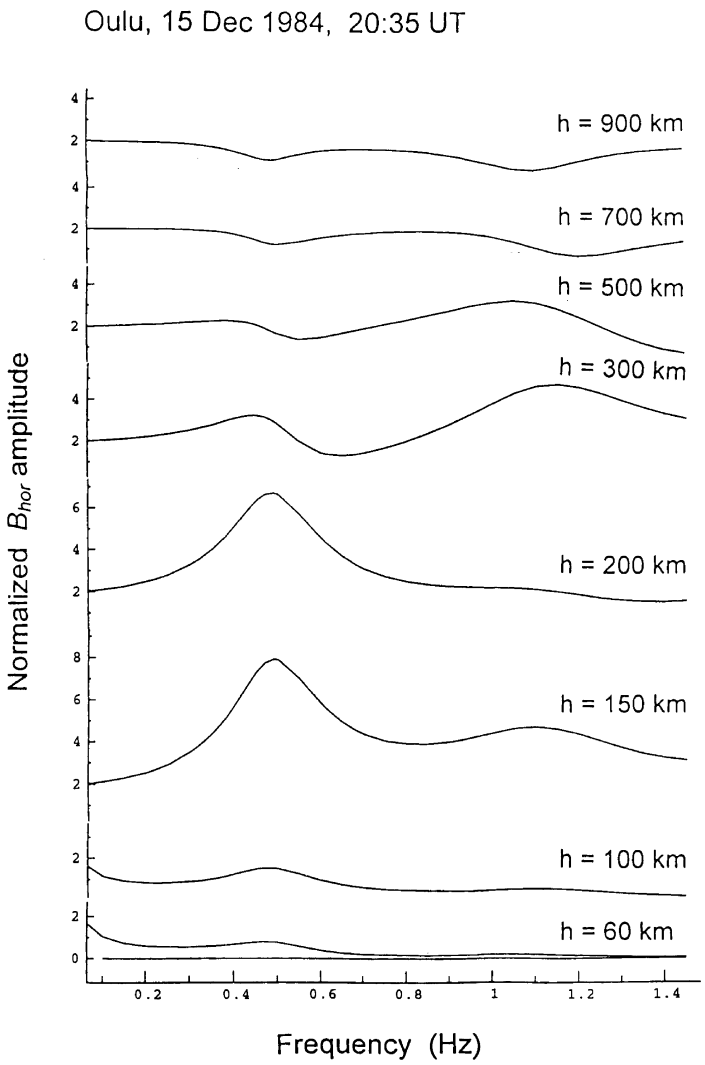

Fig. 5 (*continued*)

looking down along the **k**-vector of the incident wave mode propagating to the ground. Thus, in the northern hemisphere the **L**-polarized wave represents the ordinary Alfvén wave mode. Based on the principles mentioned by Prikner and Vagner (1991), the algorithm to compute the total wave field simulation anywhere within the ionosphere was presented by Prikner and Vagner (1995). The characteristics of the total wave field (resolved into proper wave modes) can be determined at any altitude level by solving a system of four linear algebraic equations. These equations, first presented by Vagner (1982), represent the coupling between the matrix solutions of the total field (described by means of the 4 × 4 transformation matrices **Q**) at various levels of the stratified ionosphere.

The solution at a selected frequency f and an arbitrary altitude z consists of the three Cartesian components of the complex electric $\mathbf{E}(f, z)$ and magnetic $\mathbf{B}(f, z)$ wave field amplitudes and allows the various characteristics of the total wave field to be determined. For example, the horizontal and vertical amplitudes of the total wave magnetic field (as also for the electric field) can be obtained from the complex magnetic field $\mathbf{B}(f, z)$ as follows:

$$A_{\mathrm{h}}(f, z) = \sqrt{|B_x(f, z)|^2 + |B_y(f, z)|^2}, \tag{1}$$

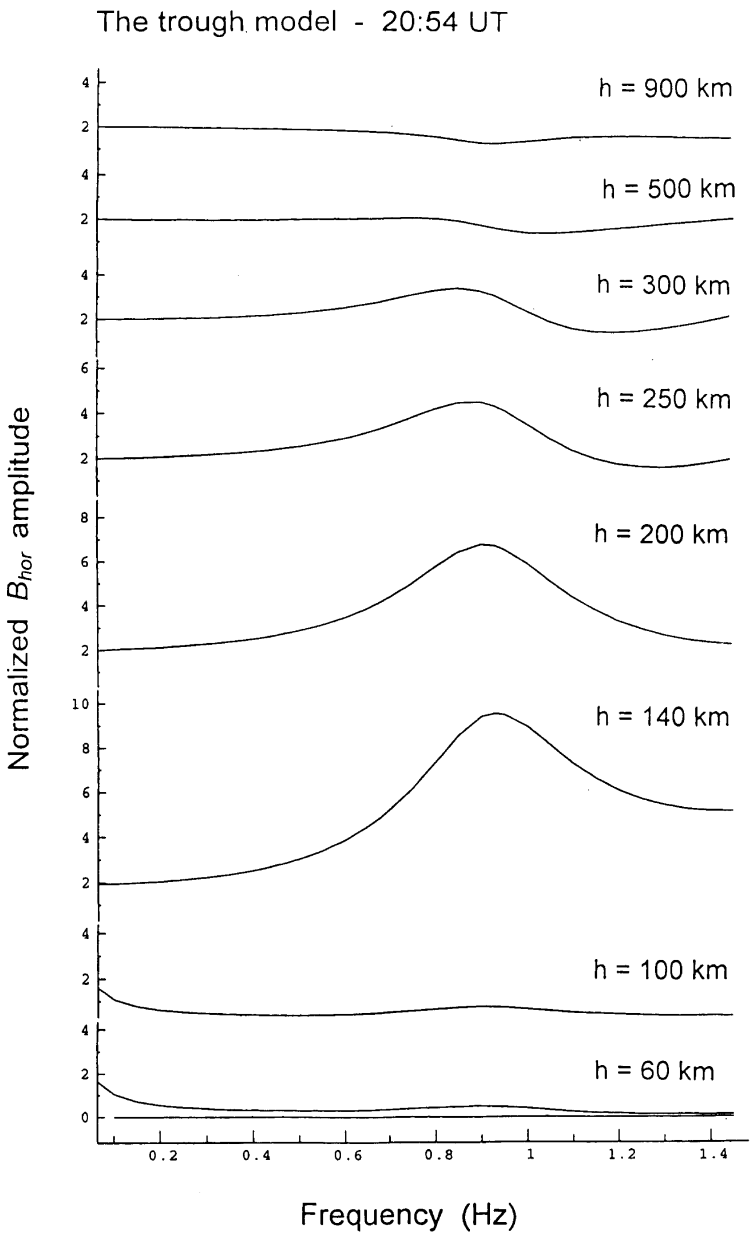

Fig. 5 (*continued*)

$$A_{\mathrm{v}}(f, z) = |B_z(f, z)|. \tag{2}$$

For practical applications, we need normalized amplitudes which are defined as the ratio between amplitudes of Eqs. (1) and (2), and the corresponding amplitudes $A^{\mathrm{inc}}_{\mathrm{h,\,v}}$ of the wave incident on the ionosphere (at altitude $z = z_{\max}$ and frequency f). These can be formally expressed as

$$TA_{\mathrm{h,\,v}}(f, z) = A_{\mathrm{h,\,v}}(f, z)/A^{\mathrm{inc}}_{\mathrm{h,\,v}}(f, z_{\max}). \tag{3}$$

Using the complex amplitudes, one can determine the various wave polarization characteristics, e.g., the sense of rotation of the polarization vector (**L** or **R**), the flattening (ellipticity) of the polarization ellipse, and deflection of the main axis of the polarization ellipse from the magnetic meridian plane (for details, see Vagner and Prikner, 1983).

Also, the electromagnetic energy flux density (i.e., the real part of the complex Poynting vector) can be calculated at different altitudes (Vagner and Prikner,

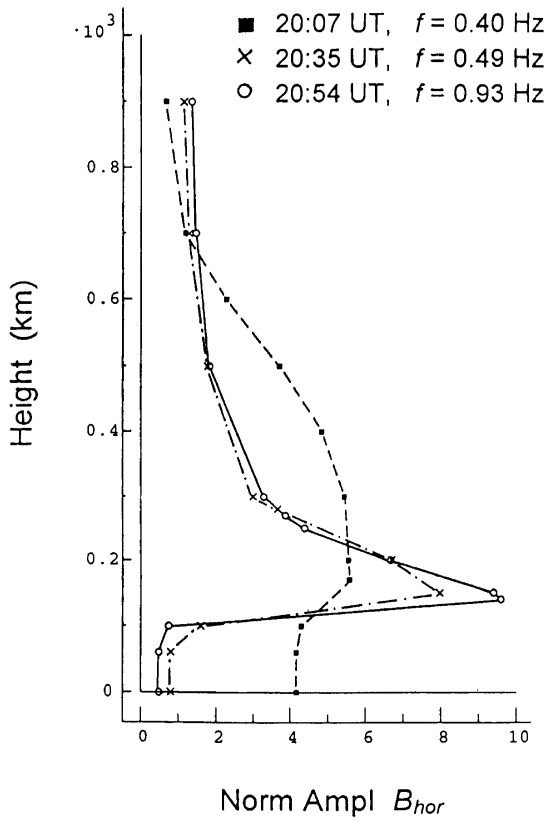

Fig. 6. The altitude profiles of the normalized horizontal wave amplitude at the resonance frequencies corresponding to the three time intervals.

1984). The gth coordinate of the real part of the Poynting vector is given by

$$\mathrm{Re}\, W_g(f, z) = \left(2\mu_0\right)^{-1} \mathrm{Re}(\mathbf{E} \times \mathbf{B}^*)_g, \tag{4}$$

where the asterisk indicates the complex conjugate, e.g., Re $W_z(f, z)$, then represents the vertical component of the energy flux density at frequency f and altitude z, and the magnitude of the energy flux density is

$$|\mathrm{Re}\, \mathbf{W}(f, z)| = \sqrt{\sum_g \left(\mathrm{Re}\, W_g\right)^2}. \tag{5}$$

Since the total energy flux density vector Re **W** does not, in general, lie in the magnetic meridian plane, the declination angle φ can be defined as an angle between the y-axis (defined to be the magnetic meridian plane) and the projection of the Re **W**-vector onto the horizontal plane (x, y):

$$\varphi(f, z) = \arctan\left(\mathrm{Re}\, W_x / \mathrm{Re}\, W_y\right), \quad \text{for Re } W_y \geq 0, \tag{6}$$

$$\varphi(f, z) = \arctan\left(\mathrm{Re}\, W_x / \mathrm{Re}\, W_y\right) + \pi\, \mathrm{sign}(\mathrm{Re}\, W_x), \quad \text{for Re } W_y < 0. \tag{7}$$

In this way, the declination $\varphi \in \langle -\pi, +\pi \rangle$ is defined as an angle from the North direction, positive to the East. The spatial orientation of the vector Re **W** is complemented by the inclination angle between the vector and the horizontal plane:

$$\Theta(f, z) = \arctan\left[\mathrm{Re}\, W_z / \sqrt{\left(\mathrm{Re}\, W_x\right)^2 + \left(\mathrm{Re}\, W_y\right)^2}\right]. \tag{8}$$

The inclination Θ is thus defined in the interval $\Theta \in \langle -\pi/2, +\pi/2 \rangle$ and, since the positive z-axis is oriented upward, Θ is positive for Re **W** directed above the horizontal plane.

In analogy with the normalized amplitude (Eq. (3)), we also define the normalized energy flux density (for frequency f and at altitude z) by

$$TW_{\mathrm{t},\,v}(f, z) = \mathrm{Re}\, W_{\mathrm{t},\,v}(f, z) / \mathrm{Re}\, W^{\mathrm{inc}}_{\mathrm{t},\,v}(f, z_{\max}), \tag{9}$$

where the indices t and v refer to the total amplitude and the vertical component, respectively.

3. Altitude profiles of wave characteristics

In P1, we analyzed a structured Pc1/IPDP event which was observed by the Finnish search coil magnetometer network on 15 December 1984. Fig. 1 depicts the observations in the D-component of the Oulu station (GGlat = 65.1°, GGlong = 25.5°, CGMlat = 61.4°, CGMlong = 105.9°; L = 4.4). As described in more detail in P1, the Pc1 pearl chain with average frequency 0.3–0.4 Hz developed, after the substorm onset at about 2030 UT, to a structured IPDP event with average frequency reaching up to 0.9 Hz, at the end of the event at 2100 UT.

As discussed in P1, the EISCAT incoherent scatter radar was scanning the mid- to high-latitude ionosphere along the magnetic meridian during part of the Pc1/IPDP event time. We used these radar measurements in P1 to calculate the ionospheric resonator properties around the Oulu station for a few times when the radar was measuring the relevant mid-latitude ionosphere. Fig. 2 depicts the altitude profiles of the electron density N_e up to 1000 km for two times (2007 and 2035 UT) when the radar was operating, and another, later time (2054 UT) where we have modeled the ionosphere with a simple trough-like profile. We note that the electron density is the controlling parameter for the resonator properties of Alfvén waves. Accordingly, the high-altitude slope of the density profile outside (or in absence of) the region of direct radar measurements was adjusted so that the

resonator eigenfrequency would better coincide with the wave frequency observed simultaneously.

Moreover, in order to determine the ionospheric resonator properties in detail, it is necessary to know the vertical profiles of the effective collision frequencies of electrons (CF_e) and ions (CF_i) with neutral particles, as well as the profile of the effective ion mass (M_i) in the ionosphere. The profiles of the collision frequencies are shown in Fig. 3 for the same times as the electron density profiles depicted in Fig. 2. As in Fig. 2, the results for the first two times are based on EISCAT data, and the third on a model. The altitude profile of the effective ion mass, shown in Fig. 4, is based on the results by Krinberg and Taschilin (1984).

We have assumed an **L**-polarized Alfvén plane wave of frequency f incident upon the upper boundary of the ionosphere at $z_{max} = 1000$ km with $\mathbf{k}||\mathbf{B}0$. For the Oulu region, the inclination of $\mathbf{B}_0$ is about -70° (downwards). The other constants necessary for modeling the wave with the matrix procedure (Prikner and Vagner, 1983, 1991) are the Earth's magnetic dipole moment, $M_E = 8.17 \times 10^{22}$ Am^2, the specific conductivity of the Earth's surface, $\sigma_E = 10^{-2}$ S/m, and the altitude stratification of the ionosphere, $\Delta z = 10$ km.

3.1. Frequency and altitude dependence of the horizontal wave field

The normalized horizontal amplitudes of the total wave magnetic field calculated according to Eq. (3) have been depicted in Fig. 5(a)–(c) as a function of frequency at several altitudes. Fig. 5(a)–(c) correspond to the same, three times as those used in Figs. 2 and 3. Fig. 5(a)–(c) clearly show the altitude variation in the resonance structure of the horizontal wave component. In each Fig. 5(a)–(c), the resonance structure is seen at a frequency for which the minimum amplitude is found on the upper boundary of the resonator, and for which the maximum amplitude is found in the central and lower part of the resonator. These frequencies can be considered as the fundamental resonance frequencies of the changing resonator. The time development of the N_e profile depicted in Fig. 2 leads to dramatic changes in the resonance structure in Fig. 5(a)–(c). The decrease in N_e values at higher altitudes and their increase in the lower ionosphere result in the increase of the resonance frequency and the decrease of the altitude, where the maximum amplitude occurs.

Moreover, we have plotted in Fig. 6 the altitude pro-

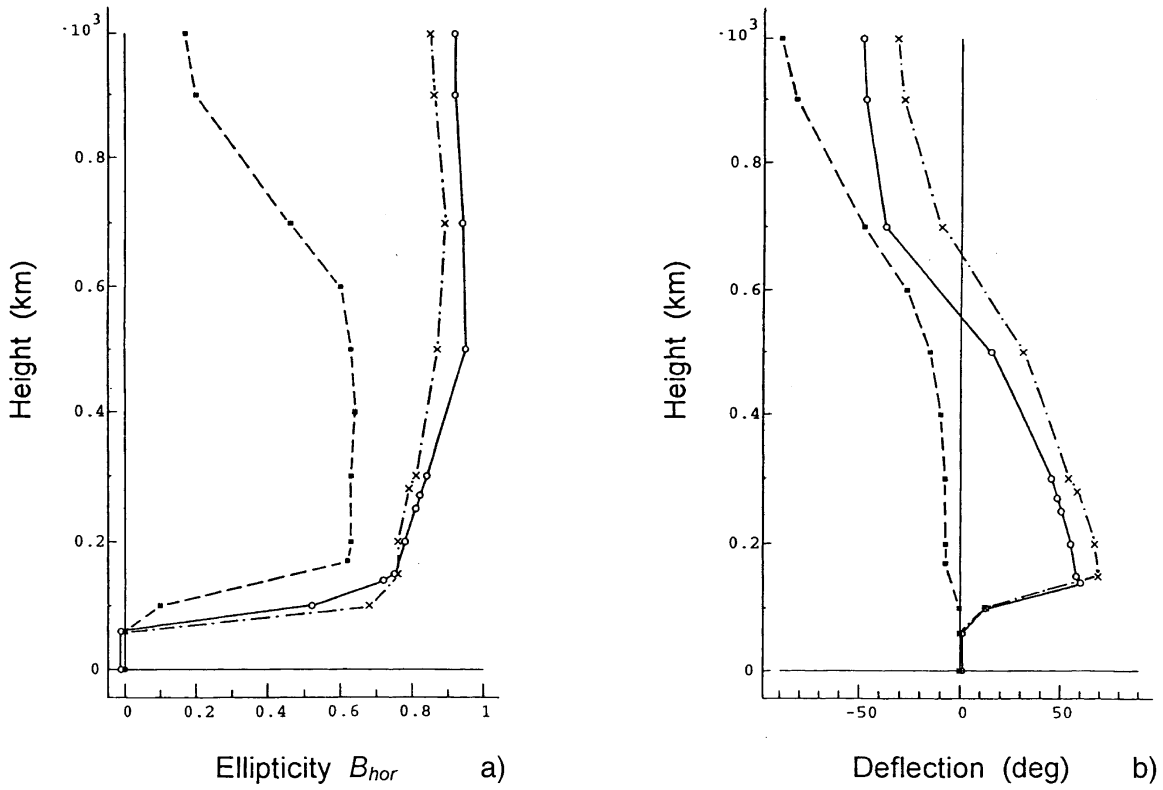

Fig. 7. The altitude profiles of: (a) ellipticity of the wave polarization ellipse in the horizontal plane and (b) deflection of the major axis of the polarization ellipse from North to East. The profiles refer to the same times and resonance frequencies as in Fig. 6(a).

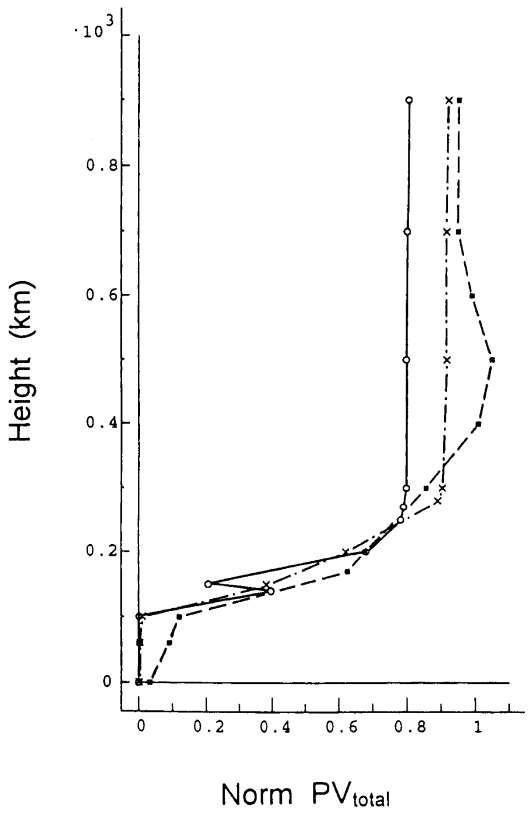

Fig. 8. The altitude profiles of the normalized energy flux density (PV) for the same times and resonance frequencies as in Fig. 6.

files of the normalized horizontal amplitude for frequencies corresponding to the eigenfrequency of the resonator at the respective three time intervals (f = 0.40 Hz at 2007 UT; f = 0.49 Hz at 2035 UT and f = 0.93 Hz at 2054 UT). During the Pc1 phase, before the IPDP event (2007 UT), the amplitude maximum at the resonance frequency is large over a wide altitude range (170–500 km), while later, during the IPDP event, the maximum amplitude region is narrower and more concentrated below 300 km. This follows from the change in the electron density profile depicted in Fig. 2, and this decrease indicates a shortening of the resonator's fundamental wave length.

3.2. Wave polarization characteristics

Similarly, we have calculated the ellipticity (defined as the ratio of the major to minor axis of the polarization ellipse), sense of rotation (**L** or **R**) of the polarization vector and deflection of the main axis from the magnetic meridian plane at the resonance frequencies for the three time intervals. The three altitude profiles of ellipticity are shown in Fig. 7(a). The positive values practically within the whole resonator indicate that the ordinary left-hand (**L**) polarized Alfvén wave persists during the wave propagation through the ionosphere. A change to a right-hand (**R**) polarized wave (negative ellipticity values) has only been found for the 2054 UT-model below the ionosphere, i.e., below 60 km. The main feature in the time development of the ellipticity profile is the fact that the ellipticity becomes nearly circularly polarized inside the resonator during the IPDP development. A sharp drop of ellipticity is seen below the ionosphere, and a linear polarization in the magnetic meridian plane is obtained on the ground.

The height profiles of the deflection of the polarization ellipse axis from the magnetic meridian plane are shown in Fig. 7(b). A clear difference is seen between the profiles before and during the IPDP phase. In the pre-IPDP model (2007 UT), the Alfvén **L**-wave has the main polarization axis practically perpendicular to the magnetic meridian plane at the upper ionospheric boundary. Within the ionospheric resonator, the westward deflection smoothly decreases and approaches the meridian plane in the lower ionosphere and on the ground. In the two other cases during the IPDP phase (2035 UT and 2054 UT), the deflection changes from West to East, reaching its eastward maximum close to the amplitude maximum. The counterclockwise rotation of the polarization axis below the E-layer of the ionosphere has been numerically predicted earlier (Nishida, 1964; Hughes, 1974).

3.3. Altitude profiles of the energy flux density

Using Eqs. (4), (5) and (9), we have calculated the altitude profiles of the normalized energy flux densities at the resonance frequencies in the three models. The results are shown in Fig. 8. High in the ionosphere (above 300 km), the energy flux is not markedly damped. Attenuation rapidly increases in the E–F1 region. Below the ionosphere and on the ground, the energy flux density is only a small fraction of the original value (of the order of 10^{-2}–10^{-4} at the end of the IPDP). The higher damping of the energy flux density during the IPDP phase at high altitudes (see Fig. 6) is due to the increased damping in the lower ionosphere when the electron density there is increased. In such a case, waves reflected from the ground back to the ionosphere are more damped and contribute less to the total resonance effect.

Fig. 9 depicts the altitude profiles of the declination and inclination of the normalized energy flux density vector for the three cases at the corresponding resonance frequencies. Through a large part of the high-altitude resonator, the energy flux vector is strongly directed downward (large negative inclination values

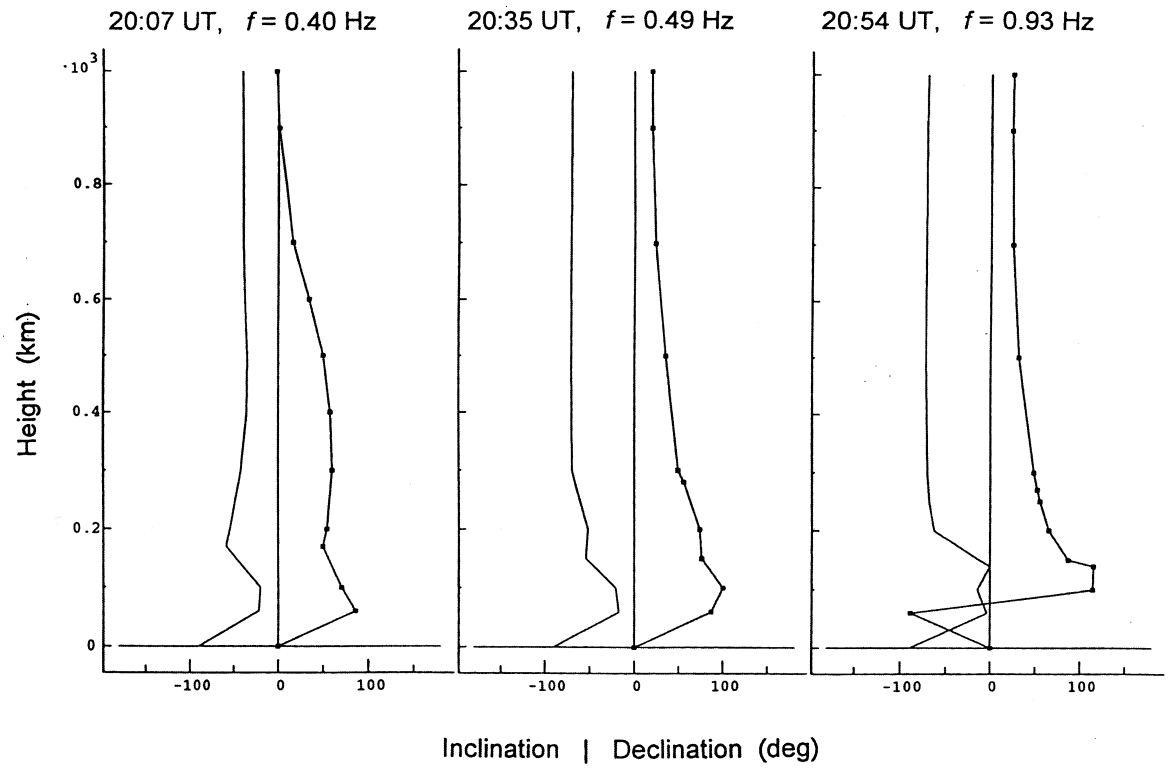

Fig. 9. The altitude profiles of the inclination (smooth line; left side in each panel; negative values earthward) and declination (smooth line with marks; right side in each panel; positive values eastward) angles of the energy flux density vector.

and only moderate declination), declining slightly to the East from the magnetic meridian plane. Great changes are found in the low ionosphere below 200 km. There, due to the decreasing absolute value of inclination and increasing declination, the energy flux vector turns, rather sharply, nearly eastward. Simultaneously, its magnitude decreases rapidly (see Fig. 8). These characteristics indicate a conversion of wave energy to horizontal propagation in this altitude range, as earlier studied by Greifinger and Greifinger (1968) and Altman and Fijalkow (1980) (see also Prikner and Vagner, 1985). However, despite the small absolute values of inclination at some altitudes, the energy flux density vector is always directed downward (below the horizon), and never upward.

4. Conclusions

This paper and its companion paper (Mursula et al., 2000; P1) study the effect of the ionospheric Alfvén resonator on a structured Pc1/IPDP wave event observed on 15 December 1984. The purpose of the present paper has been to provide additional information on the methods used in P1, as well as to present a more detailed description of the calculated properties of the waves at different altitudes of the resonator and at three different times of the Pc1/IPDP wave event.

In particular, we have demonstrated the altitude structure of the total wave inside the resonator, including its polarization properties. Moreover, we have studied the changes in wave characteristics due to changes in the local ionospheric plasma profiles during the Pc1/IPDP event. The most important parameter affecting the resonator is the electron density (N_e) profile. In P1, we used three different N_e profiles (two profiles measured by EISCAT; one model profile) to demonstrate how the resonator eigenfrequency increases due to changes in the ionospheric plasma distribution (density depletion at high altitudes and density increase at low altitudes; Bauske et al., 1997). This increase in resonator eigenfrequency was found in P1 to correspond well to the increase of the wave frequency observed on ground during the IPDP phase. During the IPDP development, the resonator eigenfrequency increases due to the decrease in resonator dimensions (shortening of the effective resonance wavelength). Moreover, the above mentioned changes in the ionospheric plasma distribution support the observation

(Kleimenova et al., 1995) that the ionospheric trough is often found above the region of observation of an IPDP event.

Studying the orientation (and size) of the energy flux vector at different ionospheric altitudes, we have shown that favorable conditions for horizontal ducting of waves (Greifinger and Greifinger, 1968; Altman and Fijalkow, 1980) seem to appear in the lower part of the resonator below about 200 km. Horizontal ducting allows the waves to propagate away from the ionospheric footpoint of the source field line. Horizontal ducting of Pc1 pulsations has been observed in several studies. However, a more accurate modeling of horizontal propagation is outside the scope of the method applied here.

Although the vertical profiles of the IAR were modeled using realistic vertical profiles of the ionospheric plasma parameters, some idealized assumptions were made. For example, we assumed an **L**-polarized, homogeneous plane wave incident upon the upper ionosphere. Taking the incident wave with a fixed frequency, we studied the ionospheric response. Then, varying the wave frequency, we obtained the complete spectral response of the IAR. However, when dealing with natural Pc1/IPDP pulsations, one should take into account nonlinear and inhomogeneous effects due to a wave packet consisting of a bunch of **k**-vectors and frequencies. Although an important task, this is clearly outside the scope of the present paper. Moreover, the good match between the observed wave frequency and the modeled resonator frequency even in the present, simplified case suggests that the frequency response of the resonator does not dramatically change in a more realistic case of waves consisting of a rather broad bunch of **k**-wave vectors and frequencies.

Finally, we would like to note that observations of large-amplitude (5–30 nT) Pc1 pulsations in the ionospheric F-region near the plasmapause by the Magsat satellite (Iyemori and Hayashi, 1989), may support the role of the ionospheric resonator amplifying waves at certain frequencies and altitudes. Amplitudes measured on the ground were more than two orders of magnitude smaller than those observed simultaneously by the Magsat satellite.

Acknowledgements

The authors wish to thank to P. Pollari for providing the EISCAT data. K. Mursula, J. Kangas, R. Kerttula, and T. Pikkarainen gratefully acknowledge the financial support by the Academy of Finland. O. A. P acknowledges the support of the International Space Science Institute (ISSI) at Bern, Switzerland, within the project "Small Alfvénic Structures in the Magnetosphere".

The EISCAT Scientific association is supported by the Suomen Akatemia of Finland, Centre National de la Recherche Scientifique of France, Max-Planck Gesellchaft of the Federal Republic of Germany, National Institute of Polar Research of Japan, Norges Almenvitenskapelige Forskningsråd of Norway, Naturvetenskapliga Forskningsrådet of Sweden and the Science and Engineering Research Council of the United Kingdom.

References

Altman, C., Fijalkow, E., 1980. The horizontal propagation of Pc1 pulsations in the ionosphere. Planetary and Space Science 28, 61–68.

Bauske, R., Noel, S., Prölss, G.W., 1997. Ionospheric storm effects in the nighttime E region caused by neutralized ring current particles. Annales Geophysicae 15, 300–305.

Bossen, M., McPherron, R.L., Russell, C.T., 1976. Simultaneous Pc1 observations by the synchronous satellite ATS-1 and ground stations: implications concerning IPDP generation mechanisms. J. Atmos. Terr. Phys 38, 1157–1167.

Greifinger, C., Greifinger, P., 1968. Theory of hydromagnetic propagation in the ionospheric wave guide. J. Geophys. Res 73, 7473–7490.

Guglielmi, A.V., 1974. Diagnostics of the magnetosphere and interplanetary medium by means of pulsations. Space Sci. Rev 16, 331–345.

Heacock, R.R., 1973. Type IPDP magnetospheric plasma wave events. Nature Phys. Science 246, 93–96.

Hughes, W.J., 1974. The effect of the atmosphere and ionosphere on long period magnetospheric micropulsations. Planet. Space Sci 22, 1157–1172.

Iyemori, T., Hayashi, K., 1989. Pc1 micropulsations observed by Magsat in the ionospheric F region. J. Geophys. Res 94 (A1), 93–100.

Kangas, J., Lukkari, L., Heacock, R.R., 1974. On the westward expansion of substorm-correlated particle phenomena. J. Geophys. Res 79, 3207–3210.

Kangas, J., Guglielmi, A., Pokhotelov, O., 1998. Morphology and physics of short-period magnetic pulsations — A review. Space Science Rev 83, 435–512.

Kleimenova, N.G., Kangas, J., Pikkarainen, T., Ranta, H., 1995. IPDP geomagnetic pulsations and the main ionospheric trough. Geomagn. and Aeron 35, 773–780.

Koleszar, T.W., 1989. The generation of IPDP micropulsations, with special attention to frequency shift mechanisms. Ph.D. thesis, University of British Columbia, Canada.

Krinberg, I.A., Taschilin, A.V., 1984. The Ionosphere and the Plasmasphere. Nauka, Moscow (in Russian).

Lysak, R.L., 1991. Feedback instability of the ionospheric resonant cavity. J. Geophys. Res 96, 1553–1568.

Lysak, R.L., 1993. Generalized model of the ionospheric Alfvén resonator. In: Auroral Plasma Dynamics, Geophysical Monograph 80, American Geophysical Union, 121–128.

Maltseva, N.F., Troitskaya, V.A., Selivanov, V.P., Feygin, F.Z., 1979. Fine structure of type IPDP pulsations on the

lines of force of the auroral zone. Geomagn. and Aeron 19, 344–347.

Mursula, K., Prikner, K., Feygin, F.Z., Bräysy, T., Kangas, J., Kerttula, R., Pollari, P., Pikkarainen, T. and Pokhotelov, O.A., 2000. Non-stationary Alfvén resonator: new results on Pc1 pearls and IPDP events. J. Atmos. Solar-Terr. Phys. 62(4), 299–309.

Nishida, A., 1964. Ionospheric screening effect and storm sudden commencement. J. Geophys. Res 69, 1861–1874.

Prikner, K., Vagner, V., 1983. Numerical modeling of the ionospheric filtration of an ULF micropulsation signal. Studia geoph. et geod 27, 173–190.

Prikner, K., Vagner, V., 1985. On the possibilities of horizontal propagation of Pc1 pulsations in the ionosphere. Studia geoph. et geod 29, 269–279.

Prikner, K., Vagner, V., 1991. Numerical solution to the problem of ionospheric filtration of ULF waves in the Pc1 range. The total wave field inside the ionospheric transition layer. Studia geoph. et geod 35, 90–99.

Prikner, K., Vagner, V., 1995. Algorithm of the problem of simulating the total wave field of the geomagnetic pulsation signal within the ionospheric transition layer. Studia geoph. et geod 39, 208–212.

Vagner, V., 1982. Numerical solution of ionospheric filtration of ULF waves. Part I: Method. Travaux Géophysiques XXX (576), 199–229.

Vagner, V., Prikner, K., 1983. Polarization characteristics of ionospheric filtration of ULF waves. Studia geoph. et geod 27, 285–297.

Vagner, V., Prikner, K., 1984. Energy characteristics of ULF wave propagation through the ionosphere. Part II: absolute directional characteristics of the energy flux density. Travaux Géophysiques XXXII (599), 387–403.